Materials Science & Engineering C 120 (2021) 111740

Contents lists available at ScienceDirect

Materials Science & Engineering C

journal homepage: www.elsevier.com/locate/msec

Hemostatic performance and biocompatibility of chitosan-based agents in experimental parenchymal bleeding

V. Deineka [a], O. Sulaieva [b], N. Pernakov [a], J. Radwan-Pragłowska [c], L. Janus [c], V. Korniienko [a], Ye Husak [a], A. Yanovska [a], I. Liubchak [a], A. Yusupova [a], M. Piątkowski [c], A. Zlatska [e,f], M. Pogorielov [a,d,*]

[a] Medical Institute, Sumy State University, Ukraine
[b] Laboratory of Pathology CSD Health Care, Ukraine
[c] Faculty of Chemical Engineering and Technology; Cracow University of Technology, Poland
[d] NanoPrime, Poland
[e] Biotechnology Laboratory Ilaya Regeneration, Medical Company Ilaya, Kyiv, Ukraine
[f] State Institute of Genetic and Regenerative Medicine of NAMS of Ukraine, Kyiv, Ukraine

ARTICLE INFO

Keywords:
Chitosan
Biodegradation
Hemostasis
Electrospinning
Aerogel
Biocompatibility

ABSTRACT

The uncontrolled parenchymatic bleeding is still a cause of serious complications in surgery and require new effective hemostatic materials. In recent years, numerous chitosan-based materials have been intensively studied for parenchymatic bleeding control but still require to increased safety and effectiveness. The current research is devoted to new hemostatic materials made of natural polymer (chitosan) developed using electrospinning and microwave-assisted methods. Hemostatic performance, biocompatibility, degradation, and in-vivo effectiveness were studied to assess functional properties of new materials. Chitosan-based agents demonstrated considerable hemostatic performance, moderate biodegradation pace and high biocompatibility in vitro. Using the electrospinning-made chitosan-copolymer significantly improved in vivo biocompatibility and degradation of Chitosan-based agents that provides opportunities for its implementation for visceral bleeding management. Chitosan aerogel could be effectively applied in hemostatic patch development due to high antibacterial activity but it is not recommended for visceral application due to moderate inflammatory effect and slow degradation.

1. Introduction

The parenchymal organs are mostly vulnerable in blunt abdominal trauma. Despite progress in surgical methods of hemostasis, the liver damages still a significant difficulty in surgery, and about 80% of isolated penetrating liver injuries can successfully be treated using non-operative management [1]. It has become the standard of using continuous observation or angioembolization [2]. But uncontrolled bleeding in high-grade hepatic injury (Organ Injury Scale IV-V grade) causes death in 42–49% in the first 24 h after admission and about 14–23% of severe hepatic injuries need emergency surgery [3,4]. Liver hemostatic strategies include left lobe ectomy, resection debridement, perihepatic packing, intrahepatic balloon tamponade, or topical hemostatic agents use [5,6].

Topical hemostatic materials (THM) facilitate coagulation and prevent bleeding recurrence that are reduce operating times, decrease the volume of blood transfusion, and re-laparotomy probability [7]. The majority of THM is of a biological origin and act as active and passive agents. Active THM made of blood components (e.g., thrombin or fibrin) can directly affect coagulation mechanisms leading to rapid blood clotting. Passive THM, made of cellulose, gelatin, collagen, etc. act by absorbing plasma and aggregating blood cells that leads to the formation of a matrix for better clotting [8]. Implementation of active THMs in surgical practice has significantly improved clinical outcomes. However, their application is limited due to high cost, contamination risks, short shelf life, low portability, performance variability, and immunological side effects [9]. Despite the wide range of THM available in the medical market, there is still a necessity to develop new materials. High hemostatic performance, safety, low cost, simple preparation, excellent biodegradability, and biocompatibility are expected [10]. Collagen, gelatin, silk, and chitosan are attractive resources for further hemostatic materials development [11–13]. Chitosan (Ch), a polyaminosaccharide

* Corresponding author at: Medical Institute, Sumy State University, Ukraine.
E-mail address: m.pogorelov@med.sumdu.edu.ua (M. Pogorielov).

https://doi.org/10.1016/j.msec.2020.111740
Received 12 July 2020; Received in revised form 14 November 2020; Accepted 16 November 2020
Available online 21 November 2020
0928-4931/© 2020 Elsevier B.V. All rights reserved.

obtained by the chitin deacetylation, is the most promising material for THM due to high biocompatibility, biodegradability, flexibility, as well as antimicrobial and hemostatic activity [14]. The Ch hemostatic effects include aggregation of red blood cells, stimulation of platelets, and contact system activation with 3D-structure formation [15,16]. Ch can be modified into various forms: films, sponges, aerogels, particles, and fibers that are usable for hemostatic application [17,18].

Several hemostatic Ch-based materials approved for external clinical applications mostly for arterial bleeding control include Celox®, TraumaStat®, HemCon® Bandage, etc. [19]. In recent years, numerous Ch-based sponges have been intensively studied for parenchymatic bleeding control [20–22]. Our previous results showed the high effectiveness of Ch-impregnated gauze for arterial bleeding. We demonstrated sufficient material-blood interplay and prominent antibacterial effects of Ch-aerogel in-vitro [23,24]. Despite high in-vitro efficiency, blood sorption capacity, and low toxicity, showed in various studies, there are some drawbacks of CH-based materials reported due to the use of acetic acid as a processing solvent. Assessment of long-term in-vivo results indicated insufficient degradation and local inflammatory response. Additionally, traditional sponges are unable to retain their shape under compression due to their fragility [25]. These shortcomings stimulate new technologies implementation to improve biocompatibility and biodegradation of Ch-based materials.

Electrospinning is a versatile technique that allows to produce nanoscale fibers with various natural and synthetic polymers, including chitosan, its derivates, and copolymer mixtures [26,27]. Some studies describe electrospinning as an advanced technique for Ch-based scaffold development for skin substitutes, tissue engineering construction, artificial organs, etc. [28]. The fibrous electrospun membrane is similar to the extracellular matrix and has the advantages of high porosity with a variable pore size distribution and higher surface area ratio [29]. Previous studies demonstrated high blood clotting activity and biocompatibility of electrospun chitosan mats. However, fast degradation dismissed their exploitation in clinical practice [30]. The copolymer mixture can increase the degradation period with a minor effect on hemostatic performance. Numerous investigations showed the application of different polymers, including PLA, PLGA, and PEO, for chitosan mat reinforcement [31]. However, there is limited data about the efficacy and properties of electrospun-*co*-polymer materials [32]. This study aimed to assess the hemostatic performance, biocompatibility, and degradation of newly produced Ch-PEO-copolymer made by electrospinning compared with Ch-aerogel and conventional THM.

2. Materials and methods

2.1. Materials

Chitosan (Ch) powder with low molecular weight and 95% deacetylation degree, polyethylene oxide (PEO) powder were purchased from Glentham Life Sciences. L-aspartic acid and L-glutamic acid, 1,2-propanodiol, ethanol 95% and human lysozyme were from Sigma Aldrich, St. Louis, MO, USA.

S. aureus and *E. coli*, obtained from the Bacteria Collection of Sumy State University, were used in the experiment. All bacteriological media were taken from HiMedia (Maharashtra, India) and Alamar blue was from Invitrogen (Carlsbad, CA, USA). For the cell culture study, all media and reagents were purchased from Gibco®, Gaithersburg, MD, USA.

2.2. Material synthesis

Production of Chitosan Aerogel (**ChAG**) conducted under microwave-assisted conditions according to Green Chemistry principles. 0.5 g of Ch was dissolved in the aquatic solution of a mixture of l-aspartic and l-glutamic amino acids. After 30 min, 10 mL of propylene glycol was added. Microwaves radiation affected the homogeneous solution for 1 min until complete water evaporation (power = 900 W). Then the prepared solution was crosslinked for 2 min (power = 900 W). Obtained Ch hydrogels washed out with distilled water until pH = 7 from unreacted acids and lyophilized for transformed into aerogels.

Chitosan electrospun membrane (**ChEsM**) was made from the Ch-PEO solution. Ch and PEO powder (2:3 g) were dissolved separately in 100 mL of 50% acetic acid under stirring for 24 h at room temperature. The obtained solutions were mixed in proportion Ch to PEO as 1:3 with conductivity equal to 1487 μS/cm. For the electrospinning process, the Ch-PEO solution was provided in the RT-Advanced machine (Linari Engineering, Pisa, Italy) in the safe cabinet with laminar airflow. Electrospinning parameters controlled with RT-Advanced software as following: flow rate - between 0.1 and 0.3 mL/min; voltage - 17 kV and the distance between the needle and the collector - 12 cm. The rotational speed of the collector (10 cm in diameter) was 800 rpm. The obtained electrospun membrane was vacuum dried at room temperature within 12 h.

2.3. Material characterization

2.3.1. SEM

To avoid a surface charge accumulation in the electron-probe samples were covered with a thin (30–50 nm) layer of silver in the vacuum set-up VUP-5M (SELMI, Sumy, Ukraine). The SEM images of sponges were observed by FEI Inspect S50B (FEI, Brno, Czech Republic) with the Everhart–Thornley secondary electron detector. Assessment of nanofiber morphology and mesh pore analysis was measured in SEM images using DiameterJ plugin 1.018w for Fiji (distribution ImageJ 1.51 w).

2.3.2. Porosity and density measurements

Isopropanol displacement was used for defining the porosity and density of the chitosan materials. The weighted samples were placed into a known volume of isopropanol for 5 min. The volume of the impregnated samples and the rest of isopropanol were measured after removing the hemostatic material. The obtained data were used for calculation of the density (Eq. (1)) and porosity (Eq. (2)):

$$d = W/(V2 - V3) \quad (1)$$

$$p = (V1 - V3)/(V2 - V3)\cdot 100\% \quad (2)$$

where:

d—density, g/cm^3
p—porosity, %
W—the weight of the sample, g
V1—the initial volume of isopropanol, cm^3
V2—the volume of isopropanol with the immersed sample, cm^3
V3—the volume of isopropanol after sample removal, cm^3

2.3.3. Degradation and biodegradation study (in-vitro)

In vitro degradation of materials was evaluated in simulated body fluid (SBF) with pH 7.4 and ion concentrations approximately equal to those of human blood plasma. The weighed samples were immersed in a sterile solution of SBF for seven days. The samples were removed, washed with distilled water, dried and weighed every 12 h.

Biodegradation study was performed with human lysozyme is an enzyme hydrolyzing β-glycosidic bonds. Lysozyme was dissolved in sterile SBF to concentration = 10 mg/L at 37 °C to imitate natural conditions. The weighed samples were immersed in solution of lysozyme for seven days. The chitosan materials were taken out, washed with distilled water, dried and weighed every 24 h. Degradation and biodegradation were calculated using the following equation:

$$(B)D = (W_0 - W_t)/W_0\cdot 100\% \quad (3)$$

where:

(B)D—(bio)degradation degree, %
W_0—the initial weight of the analyzed sample, g
W_t—sample weight after time = t, min

All experiments were repeated three times.

2.4. Antibacterial efficiency

Antibacterial activity of Ch-based hemostatic materials against Gram-negative *Escherichia coli* (B 926) and Gram-positive *Staphylococcus aureus* (B 918) was assessed. The samples (50 mg) were cut in aseptic conditions and put into a sterile test tube containing microorganisms at a concentration equivalent to 10^4 colony-forming unit (CFU)/mL (4 log10 CFU) suspended in 2 mL nutrient broth medium. Tubes with sterile growth medium and samples without microorganisms were used as a negative control. Samples of bacteria suspended in nutrient broth medium without samples were also utilized. Examined samples and controls were incubated for 2, 4, 6, 8 and 24 h at 37 °C. Aliquots of 100 μL of a bacterial suspension from tubes were spread onto the surface of agar plates and then cultivated at 37 °C for 24 h. The surviving microorganisms were counted in log10. The test was conducted in triplicate.

2.5. Cell viability assay

U2OS cell lines were obtained from the Umeå University (Sweden) and cultured in Dulbecco's modified Eagle's medium/Nutrient Mixture F-12 (DMEM, Gibco, USA) supplemented with 10% fetal bovine serum, 100 units/mL penicillin, 100 μg/mL streptomycin, 2.5 μg/mL amphotericin B (Gibco, USA) under the condition of 37 °C, 5% CO2. The cells were seeded in 24-well plates at a density of 2×10^4 cells/well. After 12 h incubation, the chitosan samples (40 mg) were added to the cells in each well. After 24 h 100 μL (10% of the volume of medium) of Alamar blue solution was added in each well. Wells containing only cells and medium without samples were used as a control. The plates were incubated for 4 h at 37 °C in the darkness. 100 μL medium from each well was transferred to another 96-well plate, and the absorbance was measured using a Multiskan FC (Thermo Fisher Scientific, Waltham, MA, USA) plate reader at wavelengths of 570 and 600 nm. The Alamar Blue test was repeated on 3rd and 7th day, with three replicates for each sample.

For Live/Dead staining ADSCs were isolated from the lipoaspirate by enzymatic digestion in 0.1% collagenase IA and 0.1% pronase with 2% fetal bovine serum (FBS) (all - Sigma-Aldrich, USA) for 1 h at 37 °C. The experiments with use of human cell culture in vitro were carried out in accordance with the human experiment issues of the Code of Ethics of the World Medical Association (Declaration of Helsinki). In all cases the voluntary informed consents were signed by donors of ADSCs. The obtained cell suspension was transferred to 25 cm^2 cell culture flask (SPL, Korea) and cultured in the following control growth medium: modified MEM-α (Sigma-Aldrich, USA) with 10% FBS (Sigma-Aldrich, USA), 2 mM L-glutamine, 100 U/ml penicillin, 100 μg/mL streptomycin and 1 ng/mL bFGF-2 (all from Sigma-Aldrich, USA). The cells were cultured in multi-gas incubator CB210 (Binder, Germany) at +37 °C in the atmosphere of saturated humidity, 5% CO_2 and 5% O_2.

For the cytotoxicity assessment, the cells were seeded on scaffolds at a density of 2×10^5 cells per 1 scaffold. After 2 days (48 h) samples were stained with PI (propidium iodide) (Sigma-Aldrich, USA) and FDA (fluorescein diacetate) (Sigma-Aldrich, USA). The number of dead and living ADSCs in different groups was counted using fluorescence microscopy (FITC and Texas Red filters; Carl Zeiss, Germany) and ZEN 2012 software.

2.6. Blood interaction test

The chitosan hemostatic materials with weight 40 mg were placed to Becton Dickinson Vacutainers® with 3.6 mg EDTA of 2 mL. 40 ml of whole human whole blood (WhB) was obtained from 2 human subjects volunteers by a registered nurse at the Medical Institute of Sumy State University. The study was previously approved by the Ethics Committee of Sumy State University, appropriate informed consent was obtained from all volunteers. The blood was added in each tube. Vacutainers were shaken for 10 min and all samples were removed and weighted. Blood sorption (BS) rate was calculated as follows:

$$BS = W2 - W1 \quad (4)$$

where:

W1 —initial weight (40 mg)
W2 —weight after interacting with blood, mg.

A completed blood count (CBC) test was performed with the remaining blood on the hematology analyzer CELL-DYN 3700 (ABBOTT, Irving, TX, USA) using reagents DIAGON (Budapest, Hungary). Platelet count (PLT, $\times 10^9$/L), platelet distribution width (PDW, %) and mean platelet volume (MPV, fL) were evaluated. Untreated blood was used as a control.

After weighing the samples were fixed in 2% glutaraldehyde for 2 h, then it was dehydrated in ethanol. All samples after drying were covered with a layer of silver (30–50 nm) for SEM.

2.7. In-vivo effectiveness assessment

Sixty 24-week-old male laboratory rats with body weight 250–300 g were used to estimate the performance of Ch-based materials. Animals were housed at 22 ± 2 °C on a 12 h light/dark cycle with food and water access "ad libra". The rats were divided into three groups 20 animals each. The following hemostatic materials were divided into three groups: Tachocomb® (Takeda Austria GmbH) as the standard treatment, ChAG, and ChEsM. The housing of the animals and all experimental procedures were carried out in compliance with the European Convention for the Protection of Vertebrate Animals used for Experimental and Other Scientific Purposes; Directive 2010/63/EU of the European Parliament and the Council on the Protection of Animals Used for Scientific Purposes. The procedures were approved by the Ethics Committee of Sumy State University.

The animals were anaesthetized by intraperitoneal injection of 7 mg/kg ketamine (Farmak JSC, Ukraine) and 10 mg/kg xylazine (Alfasan International B·V, Netherlands). A 2 cm midline laparotomy was made in sterile conditions. To simulate bleeding from a non-compressible irregular wound, a fully penetrating 4-mm punch biopsy was performed from the diaphragmatic surface on full-thickness left medial lobe of the liver. The hemostatic material was immediately applied to fill in the liver defect (Fig. 1). The bleeding time was evaluated after the hemostatic material application. The abdomen wound was closed with two layers of absorbable sutures.

The animals were euthanized by narcosis overdose ketamine (100 mg/kg) on days 7, 30 and 60 after surgery. The affected area of the liver with surrounding tissues was removed and proceed for histological assessment.

2.8. Histology and immunohistochemistry assay

The liver tissues were fixed in 10% neutral buffered formalin for 24 h and processed in an automatized histoprocessor (Milestone LOGOS Microwave Hybrid Tissue Processor, Milestone, Italy). Paraffin-embedded blocks were cut at 4 μm thickness (Thermo Scientific HM 340E microtome). Sections were stained with hematoxylin and eosin (HE) using Dako Cover Stainer (Agilent, USA) for routine histological evaluation. In addition, histochemical staining was used: toluidine blue (TB) staining to visualize mast cells, toluidine blue (TB) staining to differentiated collagen fibers, and Gomori's staining for reticular fibers visualization.

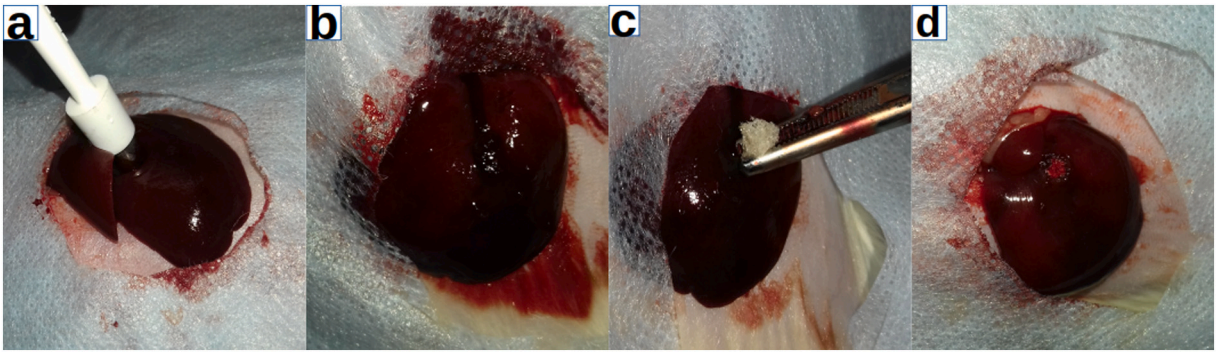


Fig. 1. Procedure of punch biopsy liver trauma (a), liver bleeding (b), hemostatic application (c) and stopped bleeding (d).

The histological analysis included assessment of tissues remodelling, progressive degradation of the material, focal proliferation, and the reaction of cellular elements responsible for degradation at the site of resection with time. The evaluation of inflammatory infiltration was performed at different terms of study, using the semi-quantitative score system. The observer scored every sample in 5 spots within the hemostatic material and around it at high magnification according to the ISO 10993-6 "*Biological evaluation of biomedical devices part 6-test for local effects after implantation*".

Immunohistochemistry (IHC) was conducted according to the standard protocol. Briefly, tissues were deparaffinized and hydrated, and endogenous peroxidase activity was blocked using 3% methanol in hydrogen peroxide. Next, antigen retrieval in a water bath at 98 °C was performed using TRIS EDTA or citrate buffer (pH 6) and followed by incubation with primary antibodies. After washing, the labeled secondary antibody (Envision Detection System, Dako) was added. The peroxidase activity was detected using diaminobenzidine (DAB) – tetrahydrochloride liquid plus Chromogen System (Dako) substrate. The reaction was stopped with distilled water, and the sections were counterstained with hematoxylin and mounted in Richard-Allan Scientific Mounting Medium (ThermoFisher). The following antibodies were used: CD68 (DAKO, Clone KP1) and CD163 (Cell Marque, Clone MRQ-26) to visualize macrophages, and Ki-67 (DAKO, Clone MIB-1) to evaluate cell proliferation.

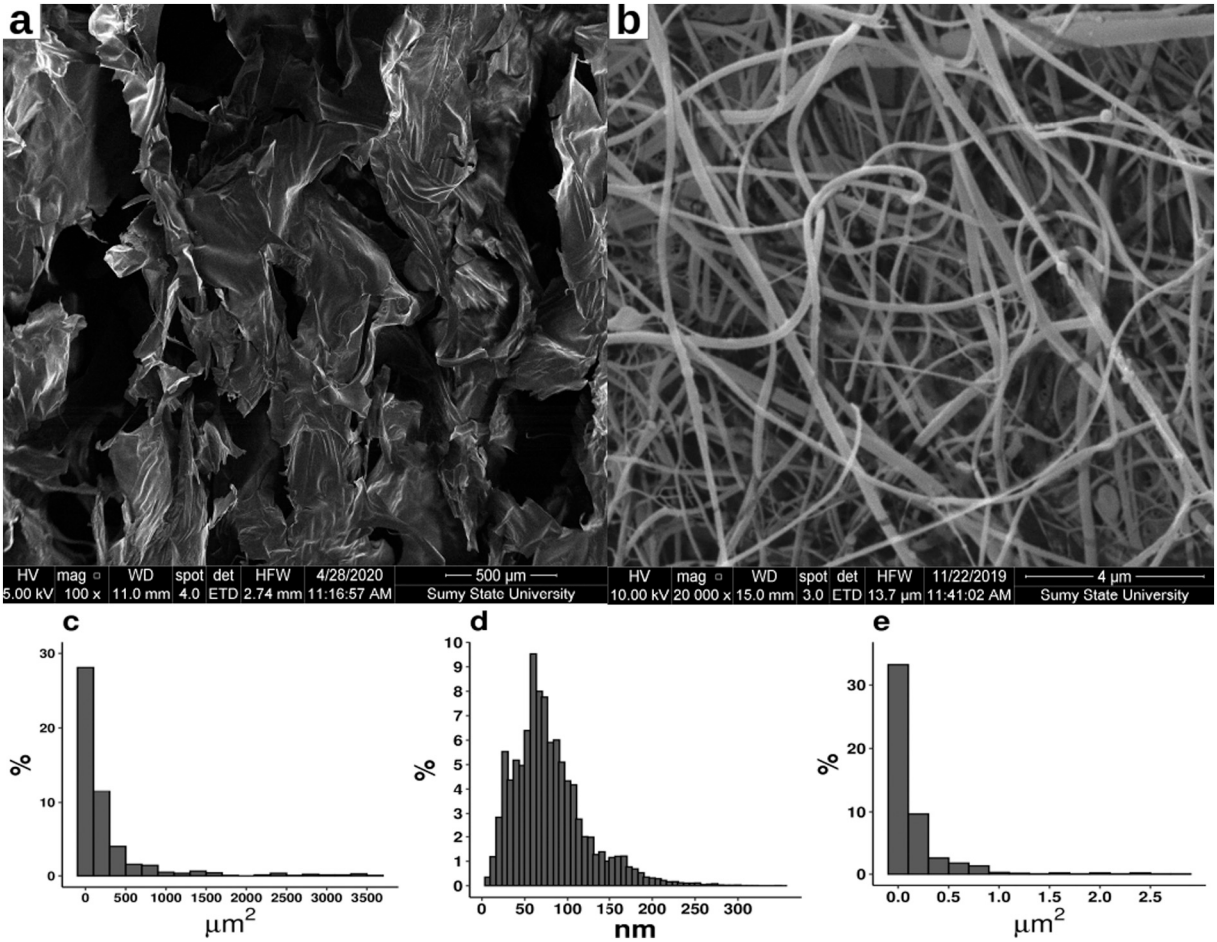


Fig. 2. Scanning electron microscopy image of ChAG (a) with analysis of pore area (c). Structures (b), pore area (e) and fiber diameter (d) of ChEsM.

2.9. Statistical analysis

The results are expressed as means ± standard deviations. Two groups were compared by *t*-test. When more than two groups were compared, ANOVA was administrated. $P < 0.05$ was considered statistically significant. Statistical analyses were performed with GraphPad Prism 8.0. and the IDE Rstudio (version 1.2.5033) for the R (version 3.4.4) software package (from http://www.rstudio.org and https://www.R-project.org).

3. Results

3.1. Structural and chemical properties

3.1.1. SEM

ChAG demonstrated a complex porous structure (Fig. 2a) with a mean pore area 414 ± 41 μm^2. Relatively uniform distribution of pores (Fig. 2c) in the micron dimension permitting fast blood absorption. However, ChAG demonstrated a low surface/volume ratio that could limit ChAG/blood cells interplay. In contrast, the ChEsM had nanofibrous architecture (Fig. 2b) of the randomly oriented fibers 180 ± 14 nm in diameter (maximum thickness – 353 ± 17 nm) (Fig. 2d). Interconnected pores between the crossing fibers were small, with an area of 0.16 ± 0.013 μm^2 and did not exceed 1 μm^2 (Fig. 2e). Such structure significantly increased the active surface area for better cell adhesion and blood sorption.

3.1.2. Porosity and density

All materials showed a high porosity that reached up to 80% with no significant differences (Fig. 3a, b) which is of great significance for hemostatic performance as guarantees better blood sorption. Also, both hemostatic materials had a very low density. But ChEsM showed significantly higher density compared to ChAG ($p < 0.05$). Both parameters depend on the technological process of material casting – lyophilization or electrospinning. Importantly, a low density can lead to faster biomaterial biodegradation after the bleeding has stopped.

3.1.3. Degradation

Fig. 3c and d demonstrates that both chitosan hemostatic agents had a similar dynamic of degradation in the SBF solution with fast primary reduction up to 40% (ChAG) or 50% (ChEsM) of their weight within the first 24 h and slowed degradation during the next days. However, the pace of ChEsM degradation was higher ($p > 0.05$), reaching 75% of weight lost on 7th day, while ChAG demonstrated only 65% of mass loss ($p < 0.05$).

Samples immersion in lysozyme showed a much higher pace of weight loss compared with the SBF that can be related to specific enzymatic degradation of chitosan. Both hemostatic materials lost more than 50% of their initial weight during the first 24 h. the further biodegradation led to additional weight loss up to 75% for ChAG and more than 82% for ChEsM ($p < 0.05$). Notably, the moderate rate of degradation is essential in two aspects. On the one hand, the material should not decompose too quickly, as fast resorption increases the risk of re-bleeding. On the other hand, too long degradation can lead to encapsulation and disruption of organ repair.

3.2. Antibacterial properties

Fig. 4 illustrates the antibacterial effects of Ch-based materials against *E. coli* and *S. aureus* that were assessed by the counting of survived colonies after the different time of incubation. Our results revealed the low inhibitory power of ChEsM samples against both *S. aureus* and *E. coli*. However, the number of microbial colonies in tubes with ChEsM was lower than in positive control during the first 6 h of incubation. In

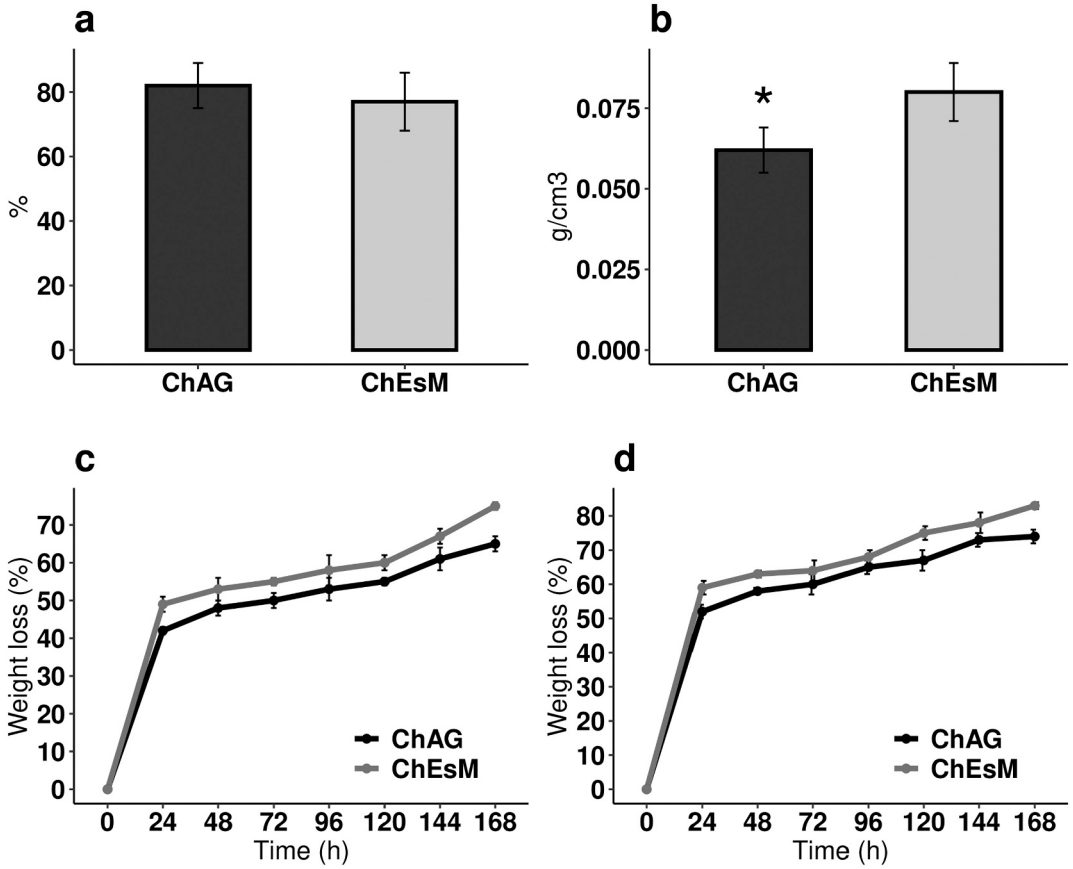


Fig. 3. The porosity (a) and density (b) of hemostatic materials (upper row) and dynamic of degradation in SBF (c) and biodegradationin in lysozyme solution (d).

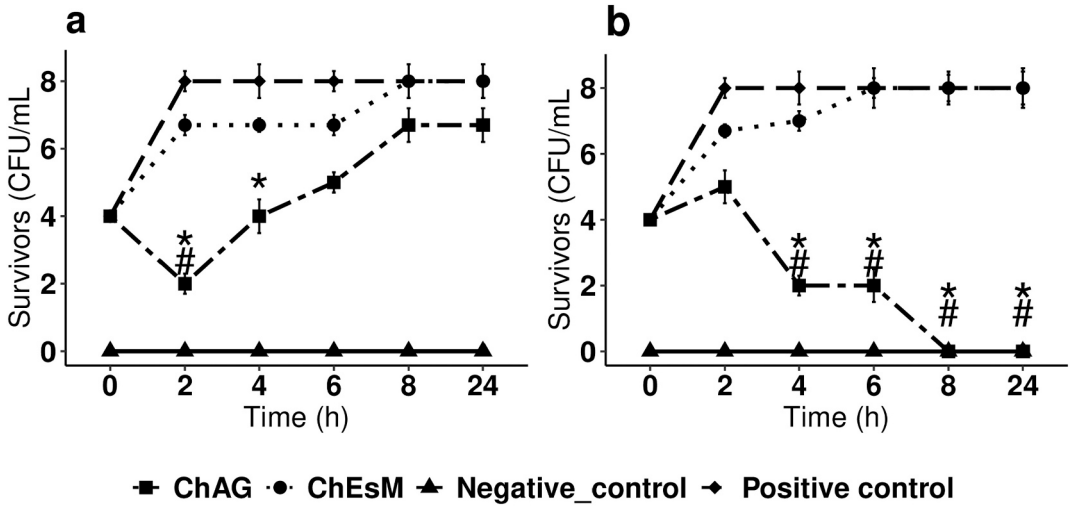


Fig. 4. Kinetics of bacterial cell amount induced by ChAG and ChEsM on *S. aureus* (a) and *E. coli* (b) "#" indicates *p* value between aerogel and electrospun groups (<0.05); "*" indicate p value between ChAG and ChEsM groups and positive control (<0.05).

contrast, ChAG displayed much higher antibacterial activity. We found out that ChAG exhibited long-lasting antibacterial activity against *E. coli*, resulting in complete growth inhibition after 24 h incubation. The antimicrobial effect of ChAG against *S. aureus* was different and demonstrated considerable inhibition during the first 2 h. However, the next period was associated with the increase of bacteria growth. Overall, ChAG was more effective against gram-negative bacteria rather than gram-positive microbes.

3.3. Cell viability assay

Resazurin reduction assay (Fig. 5b) demonstrated the same cell adhesion to both biomaterials on the first day of the study and increased cells number from day 3 of cultivation. Nevertheless, the resazurin

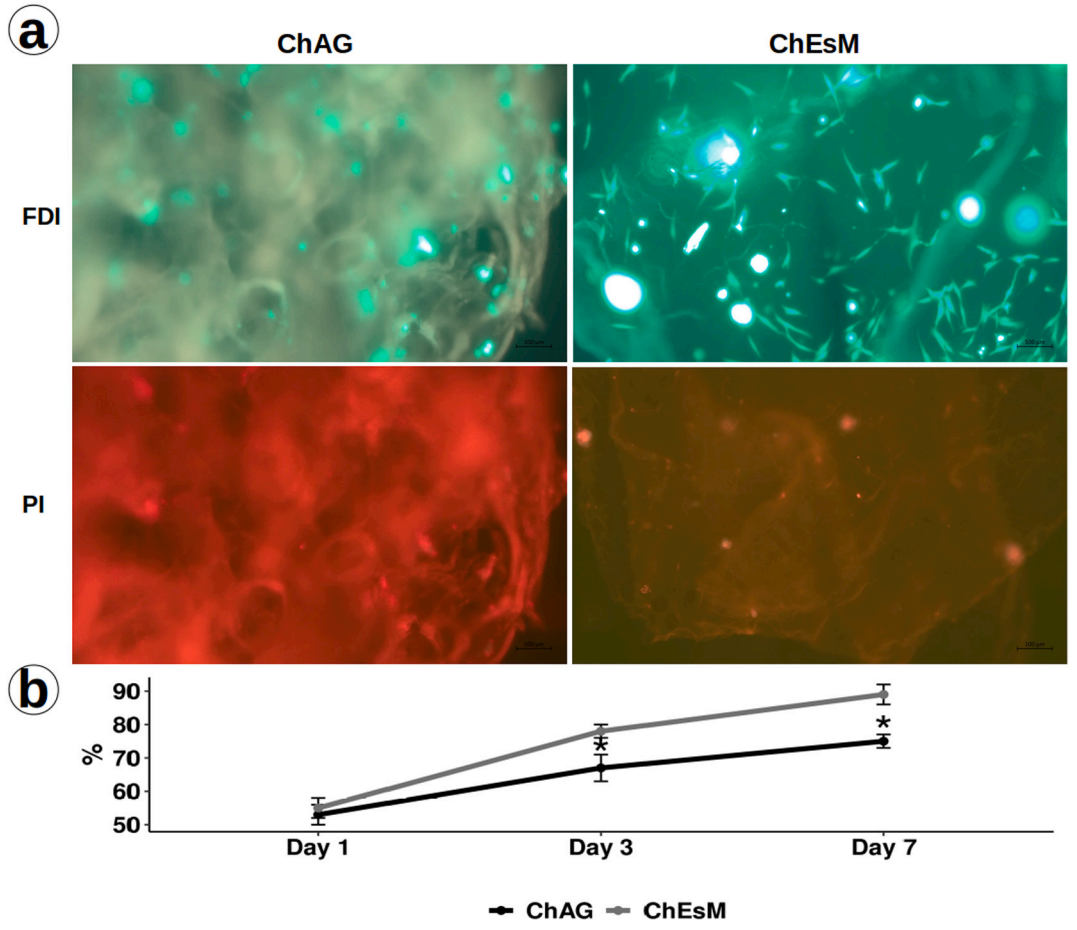


Fig. 5. a - Live/dead staining with FDA and PI after 48 h of cell cultivation. b - Cell viability using Resazurin reduction assay. *asterisks indicate *p*-value between aerogel and electrospun materials (<0.05).

reduction rate on the ChEsM was significantly higher ($p < 0.05$) on days 3 and 7, reflecting the elevated proliferation of cells.

After 48 h of cell cultivation, Live/dead staining with FDA and PI showed that most cells attached and started proliferating (Fig. 5a). The surface of the ChEsM contained more cells, while ChAG had an irregular 3D-structure with the lower number of cells attached.

The higher cells viability when incubating with ChEsM compared with ChAG can be related to both better biocompatibility of the material and/or less cytotoxicity. It seems that the fibrous architecture of the ChEsM promoted cell adhesion and proliferation so that it can serve as a tissue-engineered scaffold for improving liver repair after surgery.

3.4. Blood interaction test

Fig. 6a and b demonstrates the SEM illustration of blood interaction with hemostatic materials. There were large clusters of red blood cells and platelets on the surface of both agents — activated platelets formed a dense meshwork with fibrin fibers. Erythrocytes were firmly attached to the fibrin deposits. In addition, there were direct contacts of blood cells to electrospun fibers, that can reflect electrostatic interaction with red blood cells and stimulation of platelets.

ChAG had significantly higher ($p < 0.05$) sorption properties – it can absorb the weight of blood plasma, 25 times exceeding its own. Both Ch-based materials demonstrated prominent adhesiveness for platelets that resulted in a significant reduction of platelets number ($p < 0.05$) when interacting with blood (Fig. 6a). Also, interplay with Ch-based materials changed platelets functional parameters reflecting their activation. Contact with both chitosan materials led to a significant increase of platelets PDW and MPV when comparing to the whole blood (WhB) (Fig. 6b, c). There were no differences between the Ch-bases agents ($p > 0.05$). A change in the shape and increase in platelet volume indicates their activation as an essential step to stop bleeding.

3.5. In-vivo results

None of the animals die during the study period. The rats of all groups had no changes in health status or eating habits.

3.5.1. Bleeding times

The shortest bleeding time was in the group of Thahocomb induced complete hemostasis for 78.8 ± 5.79 s. ChAG completely stopped the bleeding for 81.33 ± 5.48 s. The mean time to complete bleeding arrest for the ChEsM was 84.53 ± 4.88 s. There were no significant differences between groups ($p > 0.05$). None of the animals needed a second application of hemostatic agents.

3.5.2. In vivo assessment of hemostatic agents' biodegradation

In one week after liver resection, an area of liver defects, filled in with biomaterials, was surrounded by a capsule separating hemostatic agents from liver tissues. Biomaterials looked, as a meshwork of branched and looped oxyphilic membranes, making a sponge-like plug. Interestingly that membranes of hemostatic agents had distinct features differing in thickness and interplay with various host cells. In group of Tachocomb, there were few cases with necrosis loci within the liver defect, filled with biomaterial surrounded by inflammatory cells (mostly neutrophils, macrophages, lymphocytes, and eosinophils). Group of ChAG demonstrated intensive inflammatory infiltration of hemostatic material and capsule around it. Whereas in Group og ChEsM, there were features of host tissues ingrowth with numerous foreign body giant cells surrounding ChEsM loops (Fig. 7). Most cases demonstrated inflammatory infiltration that was associated with varying degrees of hemostatic agent degradation.

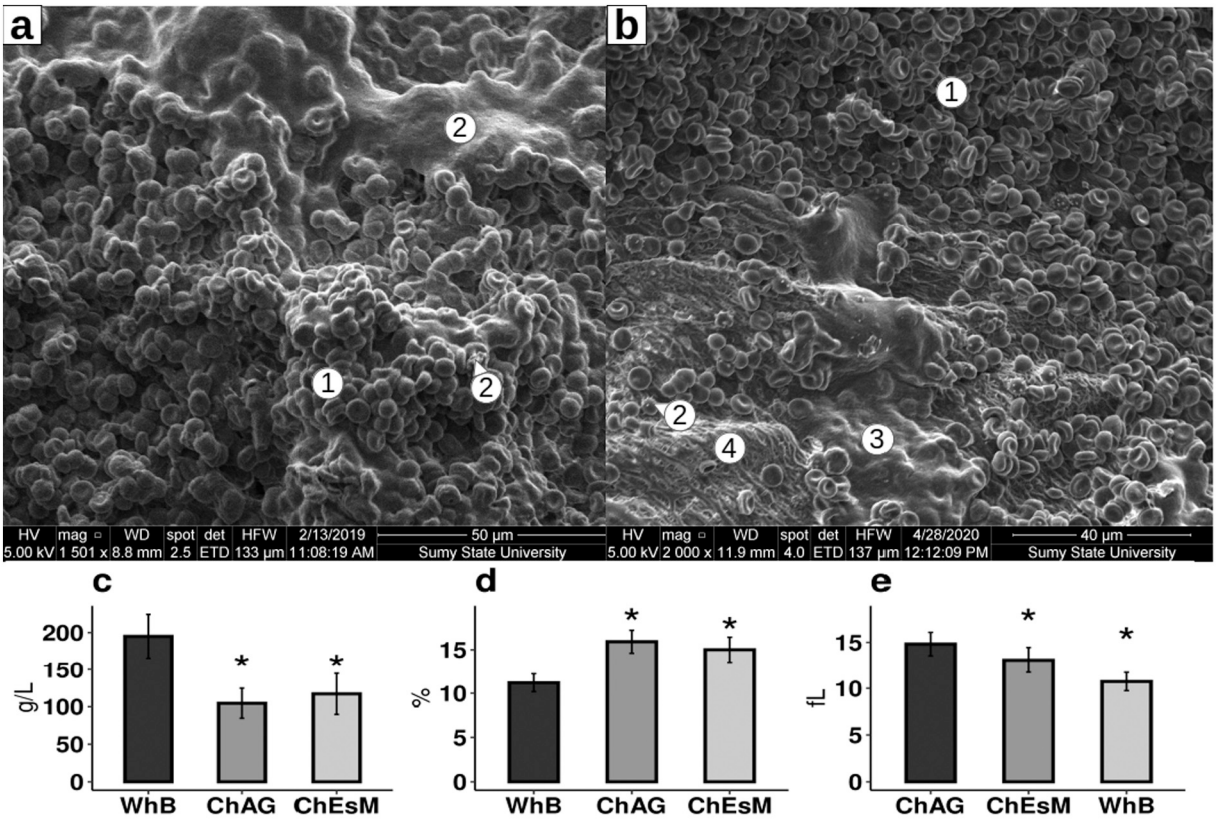


Fig. 6. SEM of ChAG (A) and ChEsM (B) interacting with blood: erythrocytes (1), platelets (2) fibrin deposition (3) and fiber of membrane (4). Blood interaction with Ch-based materials reflected in platelet (C), mean platelet volume (D), and platelet distribution width (E). *asterisks indicate p value between ChAG and ChEsM groups and whole blood control (WhB) (<0.05). Low row demonstrates.

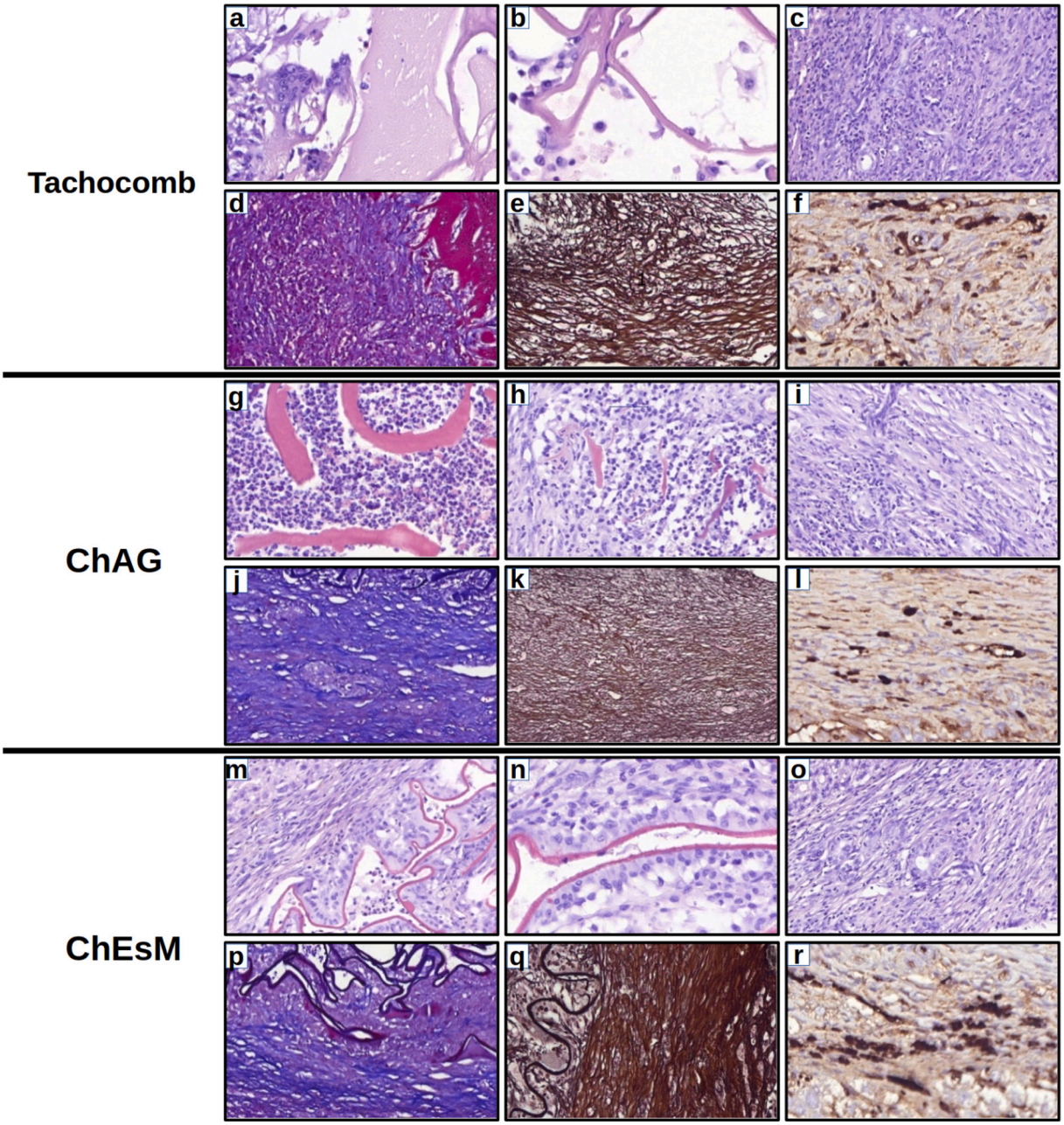


Fig. 7. Interplay between hemostatic material and host cells in animals of different groups after 7 days of the in vivo study.
In Tachocomb group, fibrin or plasm with few leucocytes (a) and foreign body giant cells (b) were within the hemostatic agent. The capsule around it contained a moderate number of leukocytes (c), with few collagen fibers (d), dense reticular fibers network (e) and a modest number of proliferating cells (f). In ChAG group was heavily infiltrated by PMN leukocytes (g) that digested biomaterial fragments (h) and infiltrated capsule around it (i). Thick capsule demarcating ChAG from liver tissues comprised a mild number of collagen and more reticular fibers (j–k) with few proliferating cells. ChEsM exhibited prominent host tissues ingrowth (m) and epithelioid-like cells adhesion (n) to ChEsM. There were a dense network of collagen (p) and reticular fibers (q) with many cholangioles and proliferating cells in the capsule. a–c, j–I, m–o – H&E staining. ×200–400. d, j, p – Masson's staining, e, k, q – Gomory's staining. ×200. f, l, r – Immunohistochemistry for Ki-67 visualizing the proliferating cells. ×400.

The size of tissue defect and dynamics of hemostatic material degradation significantly varied among animals of different groups (Table 1). In one week of the experiment, rats with ChAG had the largest size of tissue defect – its diameter was even more than the original size of injury due to abscess-like inflammatory infiltration and thick capsule formation around. In contrast, Tachocomb and ChEsM demonstrated a significant contraction of liver wound area ($P<0,001$) during the 1-st week after hemostasis, which was related to both less prominent inflammatory reaction and biomaterial degradation features.

The long-term assessment revealed the fastest pace of biomaterial degradation in Tachocomb group where the overall reduction of hemostatic agent size in about three times from week 1 to week 8 (Fig. 8). The dynamic of ChEsM degradation was comparable to Tachocomb during the first month of the experiment. However, during the second month of the study, the pace of ChEsM contraction slowed down. In contrast, ChAg showed slight changes in sponge size. The slow degradation rate was associated with fibrotic changes in capsule and surrounding tissues so that after two months of the experiment, the liver defect's diameter was equal to the initial resection volume.

Fig. 8d–f shows the size, internal structure and thickness of capsule

Table 1
Characteristics of hemostatic agent-host cells interplay in different groups.

Cells/tissues	Time points	Tachocomb	ChAG	ChEsM
Characteristics of BM -				
BM thinning and fragmentation of the BM	1 week	2	1	3
	4 weeks	2	1	2
	8 weeks	2	1	1
Host cells within BM meshwork				
PMN leukocytes	1 week	1	3	1
	4 weeks	0	3	0
	8 weeks	0	2	0
Lymphocytes	1 week	1	1	1
	4 weeks	0	0	0
	8 weeks	0	0	0
Connective tissue ingrowth	1 week	1	0	2
	4 weeks	2	0	2
	8 weeks	3	1	2
Immune cells in capsule around the BM				
Neutrophils	1 week	1	2	1
	4 weeks	0	1	0
	8 weeks	0	0	0
M1-macrophages	1 week	1	3	2
	4 weeks	1	2	1
	8 weeks	1	2	1
M2-macropahegs	1 week	3	1	2
	4 weeks	2	1	2
	8 weeks	1	2	1

around hemostatic agents in 8 weeks after surgery and hemostasis.

3.5.3. In vivo assessment of the immune response to hemostatic agents' biomaterials

The active hemostatic agent Tachocomb elicited moderate acute inflammation in the first week. Numerous polymorphonuclear leukocytes infiltrated the rests of necrotic liver cells. Inflammatory infiltration was accompanied by M1-type macrophages present in the capsule. However, their number was lower than the amount of M2-type macrophages. Numerous CD163+ cells were found at the periphery of the capsule, around areas of angiogenesis and liver cells proliferation. The liver repair was associated with cholangioles or dense cells clusters forming. At the 4th week, there were a few inflammatory cells, reflecting the resolution of the immune reaction. The capsule contained a moderate number of M1- and M2-macrophages. Degradation of biomaterial was accompanied by a sharp decline of capsule thickness and surrounding liver tissues remodelling. As a result at the 8th week, the size of the liver defect was minimal. The rests of hemostatic material contained ingrowing host tissues with foreign body giant cells participating in biomaterial resorption.

ChAG group demonstrated an acute inflammatory reaction (1 week) associated with dense polymorphonuclear cells infiltration of both central areas of ChAG sponge and the capsule around. The capsule contained a mild number of lymphocytes and numerous macrophages that were represented mostly by M1-type. Severe inflammatory reaction was associated with the thick capsule formation. Regarding liver repair, some cholangioles were present around the zone of the liver defect. However, the rate of proliferation was lower than in Tachocomb. The features of acute inflammatory reaction kept at 4th and 8th weeks, reflecting low biocompatibility of ChAG. In addition to a high number of M1 macrophages supporting inflammatory infiltration, at 4th week, the increase of M2-type macrophages was found. That was associated with the deposition of collagen in the capsule. Moreover, collagen and reticular fibers align with the biomaterial surface, generating a thick fibrotic bands at the periphery of a hemostatic plug.

In comparison with ChAG, the highly porous ChEsM biomaterial showed a significantly lower immune response during the first week. Additionally, ChEsM demonstrated high adhesiveness for the host cells that made the sheets on the biomaterial surface. The low grade of inflammatory reaction was associated with an equal number of M1- and M2-types macrophages in 1st week of the study. The acute inflammatory reaction resolved after the 4th week, which was accompanied with the intensive host tissues ingrowth inside the hemostatic sponge, capsule thickness decreases and overall liver defect reduction. Although the final ChEsM degradation was lower than Thahocomb, using electrospinning enabled Chitosan much higher biocompatibility compared with ChAG.

M2-phenotype of macrophages prevailed in the capsule of Tachocomb group animals (Fig. 9). ChAG demonstrated the highest number of proinflammatory type of macrophages with a low count of CD163+ cells. ChEsM group showed an equal amount of CD68 and CD163 in the capsule. In most cases, CD163 cells were located at the outer layer of capsule corresponding to the areas of remodelling with the feature of liver tissue repair and angiogenesis.

4. Discussion

This study showed excellent functional characteristics, effectiveness and safety of chitosan-based agents regardless of the way of their synthesis. Herein, we confirmed the high hemostatic performance of the Ch-based materials that was comparable with the active hemostatic agent of biological origin. Stop bleeding efficacy depends on biomaterial interplay with blood cells and plasma absorption. Blood interaction and hemostasis activation are the critical parameters for hemostatic materials. In vitro testing illustrated that both ChAG and ChEsM effectively interacted with platelets inducing their activation. The hemostatic effect of Chitosan includes the agglutination of blood proteins and platelet activation facilitating fibrin clot formation. As it was shown previously, the excellent haemostatic potential of Ch-based agents is due to the polycationic nature of Chitosan. It interacts easily with blood cells since plasmalemma of platelets and erythrocytes is has negatively charged. Ch-based materials stimulate platelets adhesion and aggregation that is essential for the onset of hemostasis. Besides, the amino groups (like poly-*N*-acetyl glucosamine) present in Chitosan facilitate erythrocytes aggregation [33]. Indeed, both Ch-based agents showed tight interplay with blood cells in vitro, and short bleeding time in vivo.

Moreover, both Ch-aerogel, cross-linked by L-aspartic and L-glutamic acids, and the electrospun membranes made of Ch-PEO-copolymer had high porosity that is important for blood absorption, but ChEsM demonstrated considerably higher surface-to-volume ratio. Previous research showed that nanofibrous materials exhibit high bioactivity and can reinforce hemostatic parameters [34]. However, we did not find differences in bleeding time between ChAG and ChESM.

In terms of tissues injury and bleeding, there is one more important property of Chitosan – it exhibits diverse inhibitory efficiency against different bacteria. Comparing the antimicrobial properties of Ch-based agents, we found that Ch-aerogel demonstrated significantly higher antibacterial activity against gram-negative bacteria. Some authors indicate that bacterial susceptibility is Gram-dependent and confirm that a higher inhibitory effect can be found in Gram-negative bacteria [35]. The mode of antibacterial activity is a very complicated process that varies between Gram-positive and Gram-negative bacteria, based on differences in cell structure. Gram-negative bacteria have an outer membrane that contains lipopolysaccharides providing hydrophilic surface properties. Gram-positive bacteria surface is made of peptidoglycans and teichoic acid and plays a crucial role in many membrane-bound enzymes to function [36]. The lipopolysaccharides of the outer membrane of Gram-negative bacteria containing phosphate and carboxylic groups provide the surface with a high polar character and density of negative charges. High surface charge density and hydrophilicity of bacteria support interaction and adsorption of Chitosan to the cell wall and higher growth inhibition for Gram-negative bacteria [37]. The attachment and proliferation of bacteria depend on fiber size and surface chemistry. Fiber diameter close to the bacterial length encourages the highest proliferation rates, whereas nanofibres can induce conformational changes of rod-shaped bacteria, restraining the process

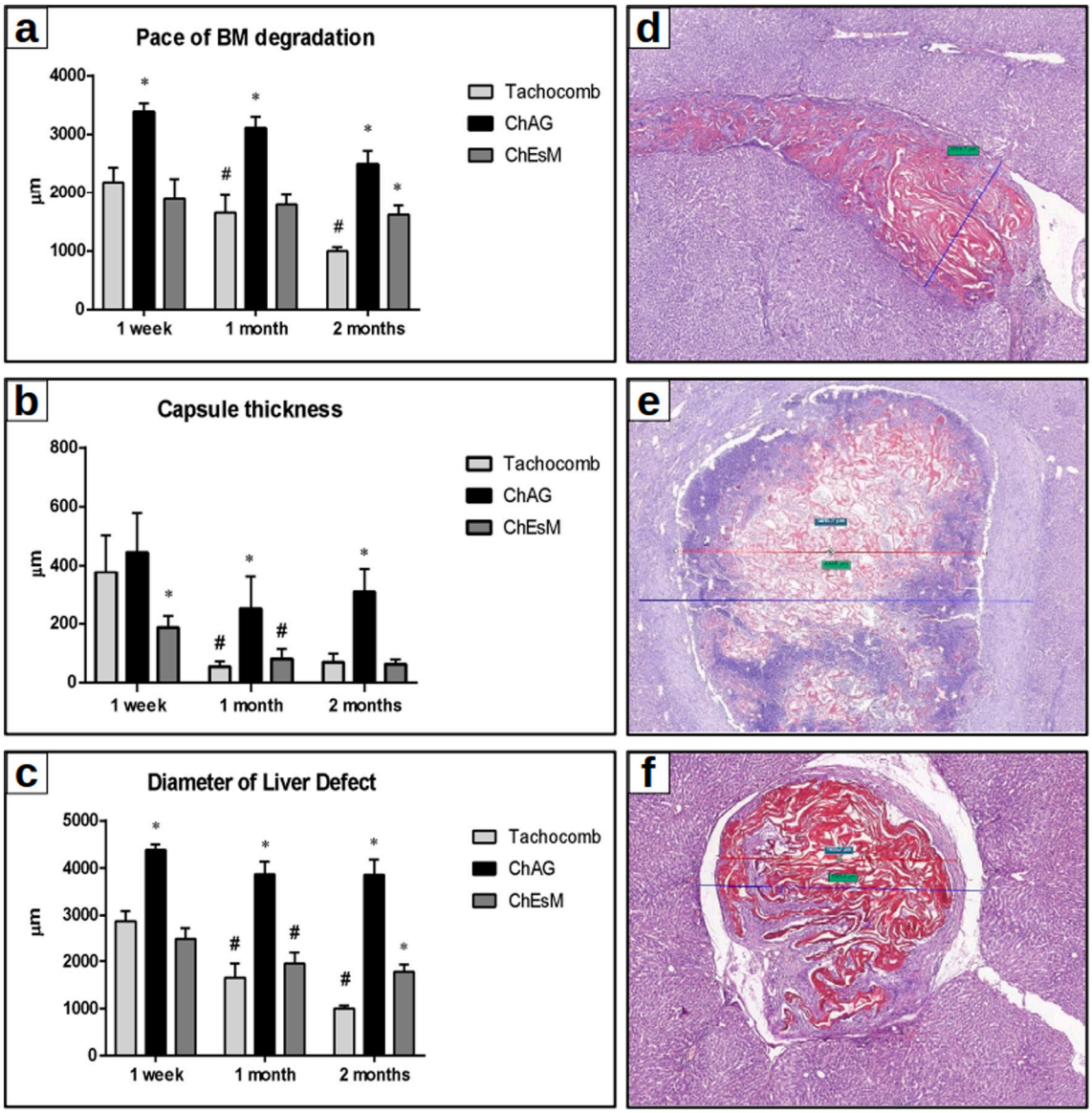


Fig. 8. The parameters of hemostatic agents' in vivo biodegradation during 2 month of the study.

of bacterial colonization [38]. Higher susceptibility of bacteria to ChAG can be due to the effect of the larger surface area of these samples that lead to high antibacterial performance [35].

Testing Ch-based agents' application for internal use, it was important to check their safety and biocompatibility. Ch-based agents demonstrated high biocompatibility in numerous studies [24,27,30]. Our in vitro tests proved biocompatibility of both ChAG and ChEsM. However, the cell proliferation rate was significantly higher in nanofibrous materials. Some data demonstrate the advantages of electrospinning for tissue engineering due to possible cell migration within the pores and connection between cell and nanofibers [39]. The differences in CgAG and ChEsM biocompatibility were even more significant during in vivo examination. While ChEsM stimulated the liver tissues ingrowth, ChAG was associated with inflammatory infiltration. Such opposite interplay between Ch-based materials and host tissues can be related with both specificity of Ch-biomaterials after processing and the nature of immunological response against them.

As it was mentioned before, Chitosan induces platelets adhesion and aggregation stimulating cot formation, immune cells activation and tissues repair. Upon activation, platelets expose various receptors on their membrane and release numerous soluble mediators that regulate inflammation, angiogenesis, and cells proliferation. Among pro-inflammatory molecules, the most important are lipid mediators (such as prostaglandins, thromboxane A2). Also, activated platelets synthesize and secrete a broad range of cytokines, including IL-1β, that facilitates the expression of adhesion molecules and chemokines expression by endothelial cells [41,42]. Moreover, platelets are the source of numerous and chemokines, such as RANTES, PF-4, MCP-1, attracting monocytes/macrophages to the place of the injury [39]. Besides, platelets contain a variety of growth factors, such as vascular endothelium growth factor (VEGF), basic fibroblast growth factor (bFGF), epidermal growth factor (EGF), angiopoietin-1 (Ang1), platelet-derived growth factor (PDGF), hepatocytes growth factor (HGF), etc. [40]. These factors are essential for both angiogenesis and liver tissues repair.

Thus, stimulating platelets activation, biomaterials can promote both inflammatory response and repair. All biomaterials can induce inflammation and foreign body reaction; however, the severity and clinical manifestation of these responses differ widely [43]. However, it seems that immunogenicity and in vivo stimulating effects of Ch-based materials was quite different, reflecting the distinct interplay of ChAG and ChEsM with immune cells and the liver cells. ChAG promoted mostly innate immunity response with active neutrophilic infiltration and M1

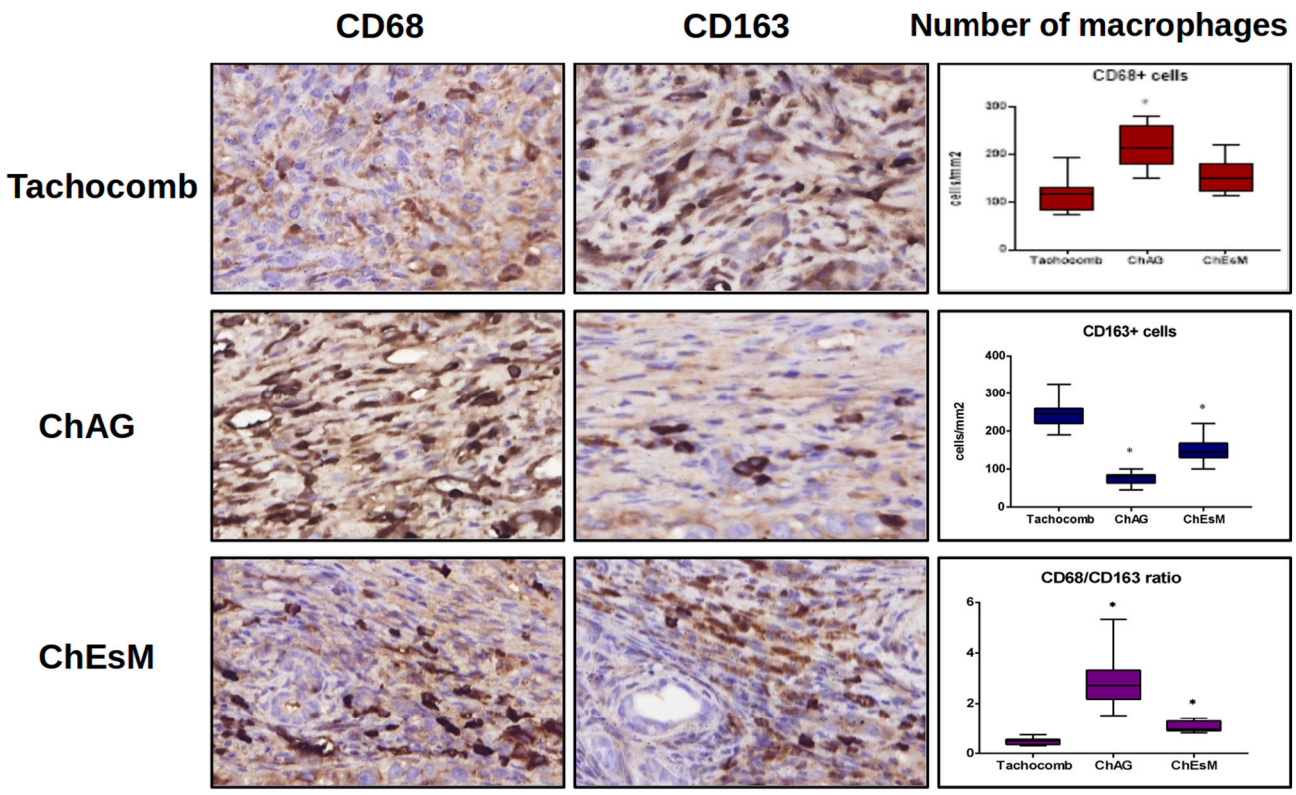


Fig. 9. The amount and spatial distribution of M1 (CD68) and M2 (CD163) macrophages in the capsule around BM-plug at different groups in 7 days after various haemostatic agent application.

macrophages activation. A severe inflammatory reaction is increasingly recognized as a crucial component influencing regeneration, and in our study, we showed that ChAG associated inflammation negatively correlated with the liver defect repair.

In contrast, ChEsM application was associated with mild inflammation and predominant activation of M2-type macrophages and accompanied with better degradation of biomaterial and improved liver repair. One of the possible mechanisms of these differences is the use of PEO as a component of Ch-copolymer within electrospun membranes. Additionally, high porosity, well-arranged nanostructure and electrostatic effects can be important for the direct interplay of electrospun membraned with host cells. The role of biomaterial architecture and physicochemical properties in defining its integrity with cells and tissues were shown in many studies [44]. Modification of PEO-containing biomaterials surface can reduce inflammatory cell adhesion and the inflammatory response [45]. Immunomodulating properties of biomaterials can be related with their effects on host dendritic cells and macrophages through modulation of cytokines secretion facilitating M2-macrophages polarization [46].

The results of our study demonstrated that physicochemical modification of Ch-based biomaterial affects its biocompartibility improving the host immune response and tissues repair.

5. Conclusion

The current research is devoted to new hemostatic materials made of natural polymer (chitosan) developed using electrospinning and microwave-assisted methods. The electrospinning significantly increases material's porosity and active surface area in contrast with Ch-aerogel that demonstrates low surface/volume ratio. Both materials show appropriate degradation and biodegradation rates that allow to apply them as hemostatic agents for parenchymatic bleeding management. At the same case, Ch-aerogel exhibit long-term antibacterial activity against *S. aureus*. Both materials demonstrate biocompatibility in experiments with U2OS cell line and human ADSCs and prominent adhesiveness for platelets that resulted in a significant reduction of platelets number when interacting with human blood. Application of both materials in liver trauma model demonstrates high effectiveness with complete hemostasis in 81.33 ± 5.48 s and 84.53 ± 4.88 s in Ch-aerogel and electrospinning membrane correspondently. Histology and immunohistochemistry assays proved that Ch-aerogel application for stopping hepatic bleeding was associated with moderate inflammatory reaction and revealed slow degradation. Electrospinning-made Ch-copolymer demonstrated high in vivo biocompatibility and degradation pace that provides opportunities for its implementation for visceral bleeding management.

Declaration of competing interest

The authors declare that they have no known competing financial interests or personal relationships that could have appeared to influence the work reported in this paper.

Acknowledgment

This research was funded by EU-H2020-MSCA-RISE, grant no 777926 "NanoSurf". Author acknowledged to to grant from Ministry of Education and Science of Ukraine, grant no 0120U101972 for support in cell culture research.

References

[1] F. Virdis, et al., Clinical outcomes of primary arterial embolization in severe hepatic trauma: a systematic review, Diagn. Interv. Imaging 100 (2) (2019) 65–75, https://doi.org/10.1016/j.diii.2018.10.004.

[2] S. Cimbanassi, et al., Nonoperative management of abdominal solid-organ injuries following blunt trauma in adults: results from an international consensus conference, J. Trauma Acute Care Surg. 84 (3) (2018) 517–531, https://doi.org/10.1097/TA.0000000000001774.

[3] D. Carver, A.W. Kirkpatrick, S. D'Amours, S.M. Hameed, J. Beveridge, C.G. Ball, A prospective evaluation of the utility of a hybrid operating suite for severely injured patients: overstated or underutilized? Ann. Surg. 271 (5) (2020) 958–961, https://doi.org/10.1097/SLA.0000000000003175.
[4] I.A. Gaski, et al., Decreased mortality, laparotomy, and embolization rates for liver injuries during a 13-year period in a major Scandinavian trauma center, Trauma Surg. Acute Care Open 3 (1) (2018) 1–6, https://doi.org/10.1136/tsaco-2018-000205.
[5] I. Afifi, S. Abayazeed, A. El-Menyar, H. Abdelrahman, R. Peralta, H. Al-Thani, Blunt liver trauma: a descriptive analysis from a level I trauma center, BMC Surg. 18 (1) (Dec. 2018) 42, https://doi.org/10.1186/s12893-018-0369-4.
[6] L.M. Kodadek, D.T. Efron, E.R. Haut, Intrahepatic balloon tamponade for penetrating liver injury: rarely needed but highly effective, World J. Surg. 43 (2) (Feb. 2019) 486–489, https://doi.org/10.1007/s00268-018-4812-6.
[7] R. Manuel G, The economic burden of bleeds and transfusions in selected surgeries: a retrospective multi center analysis from the US perspective, Am. J. Biomed. Sci. Res. 2 (5) (May 2019) 211–216, https://doi.org/10.34297/AJBSR.2019.02.000610.
[8] O. Chiara, et al., A systematic review on the use of topical hemostats in trauma and emergency surgery, BMC Surg. 18 (1) (2018) 1–20, https://doi.org/10.1186/s12893-018-0398-z.
[9] D.S.A. Hickman, C.L. Pawlowski, U.D.S. Sekhon, J. Marks, A. Sen Gupta, Biomaterials and advanced technologies for hemostatic management of bleeding, Adv. Mater. 30 (4) (2018) 1–40, https://doi.org/10.1002/adma.201700859.
[10] B. Wang, A. Johnson, W. Li, Development of an extracellular matrix<unicode>8208</unicode>enriched gelatin sponge for liver wound dressing, J. Biomed. Mater. Res. Part A (Apr. 2020), jbm.a.36965, https://doi.org/10.1002/jbm.a.36965.
[11] J.Y. Liu, et al., Hemostatic porous sponges of cross-linked hyaluronic acid/cationized dextran by one self-foaming process, Mater. Sci. Eng. C 83 (October) (2018) 160–168, https://doi.org/10.1016/j.msec.2017.10.007.
[12] Y.B. Seo, et al., In vitro and in vivo evaluation of the duck's feet collagen sponge for hemostatic applications, J. Biomater. Appl. 32 (4) (Oct. 2017) 484–491, https://doi.org/10.1177/0885328217733338.
[13] P. Slezak, C. Keibl, H. Redl, D. Labahn, H. Gulle, An efficacy comparison of two hemostatic agents in a porcine liver bleeding model: gelatin/thrombin flowable matrix versus collagen/thrombin powder, J. Investig. Surg. (Mar. 2019) 1–11, https://doi.org/10.1080/08941939.2019.1571130.
[14] M.A. Khan, M. Mujahid, A review on recent advances in chitosan based composite for hemostatic dressings, Int. J. Biol. Macromol. 124 (Mar. 2019) 138–147, https://doi.org/10.1016/j.ijbiomac.2018.11.045.
[15] Y. Wang, K. Kim, M.S. Lee, H. Lee, Hemostatic ability of chitosan-phosphate inspired by coagulation mechanisms of platelet polyphosphates, Macromol. Biosci. 18 (4) (Apr. 2018) 1700378, https://doi.org/10.1002/mabi.201700378.
[16] Z. Shariatinia, Pharmaceutical applications of chitosan, Adv. Colloid Interf. Sci. 263 (Jan. 2019) 131–194, https://doi.org/10.1016/j.cis.2018.11.008.
[17] Q. Ouyang, et al., Construction of a composite sponge containing tilapia peptides and chitosan with improved hemostatic performance, Int. J. Biol. Macromol. 139 (Oct. 2019) 719–729, https://doi.org/10.1016/j.ijbiomac.2019.07.163.
[18] T. Okada, K. Uto, T. Aoyagi, M. Ebara, A biomimetic approach to hormone resistant prostate cancer cell isolation using inactivated Sendai virus (HVJ-E), Biomater. Sci. 4 (1) (2016) 96–103, https://doi.org/10.1039/C5BM00375J.
[19] X. Huang, et al., Using absorbable chitosan hemostatic sponges as a promising surgical dressing, Int. J. Biol. Macromol. 75 (2015) 322–329, https://doi.org/10.1016/j.ijbiomac.2015.01.049.
[20] G. Lan, et al., Chitosan/gelatin composite sponge is an absorbable surgical hemostatic agent, Colloids Surf. B: Biointerfaces 136 (2015) 1026–1034, https://doi.org/10.1016/j.colsurfb.2015.10.039.
[21] W. Zhang, Y.-L. Sun, D.-H. Chen, Effects of chitin and sepia ink hybrid hemostatic sponge on the blood parameters of mice, Mar. Drugs 12 (4) (Apr. 2014) 2269–2281, https://doi.org/10.3390/md12042269.
[22] Z. Qian, et al., A porous sodium polyacrylate-grafted chitosan xerogel for severe hemorrhage control synthesized from one-pot reaction, J. Mater. Chem. B 5 (25) (2017) 4845–4851, https://doi.org/10.1039/C7TB00802C.
[23] M. Pogorielov, et al., Haemostatic chitosan coated gauze: in vitro interaction with human blood and in-vivo effectiveness, Biomater. Res. 19 (1) (2015) 1–10, https://doi.org/10.1186/s40824-015-0044-0.
[24] J. Radwan-Pragłowska, et al., Chitosan-based bioactive hemostatic agents with antibacterial properties—synthesis and characterization, Molecules 24 (14) (Jul. 2019) 2629, https://doi.org/10.3390/molecules24142629.
[25] P.L. Kang, et al., Development and assessment of hemostasis chitosan dressings, Carbohydr. Polym. 85 (3) (2011) 565–570, https://doi.org/10.1016/j.carbpol.2011.03.015.
[26] S. Qasim, et al., Electrospinning of chitosan-based solutions for tissue engineering and regenerative medicine, Int. J. Mol. Sci. 19 (2) (Jan. 2018) 407, https://doi.org/10.3390/ijms19020407.
[27] J. Sun, S.L. Perry, J.D. Schiffman, Electrospinning nanofibers from chitosan/hyaluronic acid complex coacervates, Biomacromolecules 20 (11) (2019) 4191–4198, https://doi.org/10.1021/acs.biomac.9b01072.
[28] S. Bayat, N. Amiri, E. Pishavar, F. Kalalinia, J. Movaffagh, M. Hashemi, Bromelain-loaded chitosan nanofibers prepared by electrospinning method for burn wound healing in animal models, Life Sci. 229 (Jul. 2019) 57–66, https://doi.org/10.1016/j.lfs.2019.05.028.
[29] R. Rasouli, A. Barhoum, M. Bechelany, A. Dufresne, Nanofibers for biomedical and healthcare applications, Macromol. Biosci. 19 (2) (2019) 1–27, https://doi.org/10.1002/mabi.201800256.
[30] Z. Hu, D.-Y. Zhang, S.-T. Lu, P.-W. Li, S.-D. Li, Chitosan-based composite materials for prospective hemostatic applications, Mar. Drugs 16 (8) (Aug. 2018) 273, https://doi.org/10.3390/md16080273.
[31] A. Barhoum, K. Pal, H. Rahier, H. Uludag, I.S. Kim, M. Bechelany, Nanofibers as new-generation materials: from spinning and nano-spinning fabrication techniques to emerging applications, Appl. Mater. Today 17 (2019) 1–35, https://doi.org/10.1016/j.apmt.2019.06.015.
[32] Y. Zhou, H. Yang, X. Liu, J. Mao, S. Gu, W. Xu, Electrospinning of carboxyethyl chitosan/poly(vinyl alcohol)/silk fibroin nanoparticles for wound dressings, Int. J. Biol. Macromol. 53 (Feb. 2013) 88–92, https://doi.org/10.1016/j.ijbiomac.2012.11.013.
[33] B.K. Gu, S.J. Park, M.S. Kim, C.M. Kang, J. Il Kim, C.H. Kim, Fabrication of sonicated chitosan nanofiber mat with enlarged porosity for use as hemostatic materials, Carbohydr. Polym. 97 (1) (2013) 65–73, https://doi.org/10.1016/j.carbpol.2013.04.060.
[34] T. Yan, F. Cheng, X. Wei, Y. Huang, J. He, Biodegradable collagen sponge reinforced with chitosan/calcium pyrophosphate nanoflowers for rapid hemostasis, Carbohydr. Polym. 170 (Aug. 2017) 271–280, https://doi.org/10.1016/j.carbpol.2017.04.080.
[35] M. Kong, X.G. Chen, K. Xing, H.J. Park, Antimicrobial properties of chitosan and mode of action: a state of the art review, Int. J. Food Microbiol. 144 (1) (2010) 51–63, https://doi.org/10.1016/j.ijfoodmicro.2010.09.012.
[36] G. Kravanja, M. Primožič, Ž. Knez, M. Leitgeb, Chitosan-based (nano)materials for novel biomedical applications, Molecules 24 (10) (May 2019) 1960, https://doi.org/10.3390/molecules24101960.
[37] M. Arkoun, F. Daigle, M.-C. Heuzey, A. Ajji, Mechanism of action of electrospun chitosan-based nanofibers against meat spoilage and pathogenic bacteria, Molecules 22 (4) (Apr. 2017) 585, https://doi.org/10.3390/molecules22040585.
[38] M. Abrigo, P. Kingshott, S.L. McArthur, Electrospun polystyrene fiber diameter influencing bacterial attachment, proliferation, and growth, ACS Appl. Mater. Interfaces 7 (14) (Apr. 2015) 7644–7652, https://doi.org/10.1021/acsami.5b00453.
[39] K. Rodríguez, J. Sundberg, P. Gatenholm, S. Renneckar, Electrospun nanofibrous cellulose scaffolds with controlled microarchitecture, Carbohydr. Polym. 100 (2014) 143–149, https://doi.org/10.1016/j.carbpol.2012.12.037.
[40] F. Eisinger, H.F. Langer, The mutual relation of platelet activation and innate immunity, Hamostaseologie 38 (4) (2018) 186–202, https://doi.org/10.1055/s-0038-1669450.
[41] O. Sulaieva, V. Deliy, S. Zharikov, Relationship between leukocytes recruitment and risk of rebleeding in patients with peptic ulcers, Pathophysiology 22 (4) (2015) 175–182, https://doi.org/10.1016/j.pathophys.2015.07.002.
[42] F. Eisinger, J. Patzelt, H.F. Langer, The platelet response to tissue injury, Front. Med. 5 (NOV) (2018) 1–15, https://doi.org/10.3389/fmed.2018.00317.
[43] W.K. Ward, A review of the foreign-body response to subcutaneously-implanted devices: the role of macrophages and cytokines in biofouling and fibrosis, J. Diabetes Sci. Technol. 2 (5) (2008) 768–777, https://doi.org/10.1177/193229680800200504.
[44] A. Vishwakarma, et al., Engineering immunomodulatory biomaterials to tune the inflammatory response, Trends Biotechnol. 34 (6) (2016) 470–482, https://doi.org/10.1016/j.tibtech.2016.03.009.
[45] C.R. J., J.M. A., Effects of surface-coupled polyethylene oxide on human macrophage adhesion and foreign body giant cell formation in vitro, J. Biomed. Mater. Res. 44 (2) (1999), https://doi.org/10.1002/(SICI)1097-4636(199902)44:2<206::AID-JBM11>3.0.CO;2-D.
[46] Laura Beth Moore, T.R. Kyriakides, Immune responses to biosurfaces, Adv. Exp. Med. Biol. 865 (10) (2015) 93–108, https://doi.org/10.1007/978-3-319-18603-0.